Structures 40 (2022) 109–126

Contents lists available at ScienceDirect

Structures

journal homepage: www.elsevier.com/locate/structures

Horizontal and vertical axis wind turbines on existing jacket platforms: Part 2 – Retrofitting activities

Paulo Mendes [a,*], José A.F.O. Correia [a], João Arrojado [a], Taemin Heo [b], Nicholas Fantuzzi [c], Lance Manuel [b]

[a] CONSTRUCT/Faculty of Engineering, University of Porto, Portugal
[b] University of Texas, Austin, USA
[c] DICAM Department, University of Bologna, Italy

ARTICLE INFO

Keywords:
Finite element method
Offshore structures
Wind turbine
Retrofitting
Conforming and nonconforming formulations

ABSTRACT

A fast-expanding number of oil & gas companies are planning to shift investment to renewable energy projects, with offshore wind expected to spearhead this campaign. Now, with global demand for wind power growing, major oil and gas companies are diversifying their portfolios by developing offshore wind and the companies that provide services to offshore fossil fuel platforms are seeing a new market rising in their wake. Changing the future service life of oil and gas platforms by converting them into support structures for offshore wind turbines requires some retrofitting measures in order to reduce the cost of maintenance, increase reliability and improve the structural performance of the integrated turbine-platform system. Five different retrofitting solutions are presented, four of which are related to the substructure and one is related to a modified wind turbine. The retrofitting solution related to the substructure was the only solution that guaranteed safety. This study dealing with the retrofitting activities is the continuation of a previous work where the repurposing of oil and gas platforms for offshore wind energy generation was investigated.

1. Introduction

Exploiting offshore resources started decades ago and was followed by a rapid growth of the offshore oil and gas industry. However, in recent years, there has been a slowdown in the industry due to a depletion of resources and greater environmental concerns and lower oil prices. Decommissioning of oil & gas platforms was assumed to be the only solution once the resources were exhausted; however, the retrofitting on these platforms to support wind turbines brings a far more sustainable solution. Different approaches for aspects of retrofitting existing platforms have been investigated to make the procedure easier. Jackets platforms have been widely used all around the world in the oil and gas industry. As a result, the conversion of jacket platforms forms the focus of this study. Alessi et al. [1] studied the initial phase of converting a jacket platform and developed a model for its structural analysis. Controlling seismic vibrations has been assessed by Komachi et al. [2] for a jacket platform in the Persian Gulf, using friction dampers to study seismic behavior. The same method was employed by Minh Le et al. [3] in another study for investigation. The material deterioration (corrosion) also needs to be adequately accounted [4] in order to maintain structural resilience [5]. In a more general case study, Morrison [6] investigated the potential reuse of North Sea installations for wind turbines. A numerical investigation has been conducted by Gao and Zhang [7] on the dynamic behavior of jacket foundations. Cheng et al. [8] also performed a numerical analysis on the dynamic response of large wind turbines. Kaiser & Snyder [9] carried out an overview of the expected workflows and stages of decommissioning that are likely to arise for offshore wind farms, described the exposure and liability of the parties involved and compared the different stages from oil and gas platform decommissioning. In the present study, as all the retrofitting processes are aimed to be after some service life of the jacket platform, fatigue analysis can be a critical issue. Many studies have been performed by researchers to analyze the fatigue performance to ease ahead of the retrofitting process. Sørensen studied the fatigue life of wind turbine grouted connections and how the load frequency affects [10]. Fatigue of grouted connections has been investigated in another study [11] by Schaumann and Raba for submerged small-scale joints Fatigue inspection and life extension of monopiles have both been investigated

* Corresponding author.
E-mail address: pjmendes@fe.up.pt (P. Mendes).

https://doi.org/10.1016/j.istruc.2022.03.084
Received 11 August 2021; Received in revised form 29 March 2022; Accepted 30 March 2022
Available online 11 April 2022

Table 1
Horizontal- and vertical-axis turbine mass matrix results.

	HAWT	VAWT
m_{1x}	278263.09 kg	278263.09 kg
m_{2x}	162534.86 kg	162534.86 kg
m_{3x}	131654.74 kg	131654.74 kg
m_{4x}	123604.06 kg	123604.06 kg
m_{5x}	1163977.30 kg	943606.10 kg
m_{6x}	856843.20 kg	710705 kg
m_{1y}	278263.09 kg	278263.09 kg
m_{2y}	162534.86 kg	162534.86
m_{3y}	131654.74 kg	131654.74 kg
m_{4y}	123604.06 kg	123604.06 kg
m_{5y}	1163977.30 kg	943606.10 kg
m_{6y}	856843.20 kg	710705 kg
J_1	68867970.64 m^4	68867970.64 m^4
J_2	24647179.72 m^4	24647179.72 m^4
J_3	12364431.90 m^4	12364431.90 m^4
J_4	7054173.79 m^4	7054173.79 m^4
J_5	3774879.46 m^4	2115500.689 m^4
J_6	1659377.2 m^4	3970550.49 m^4

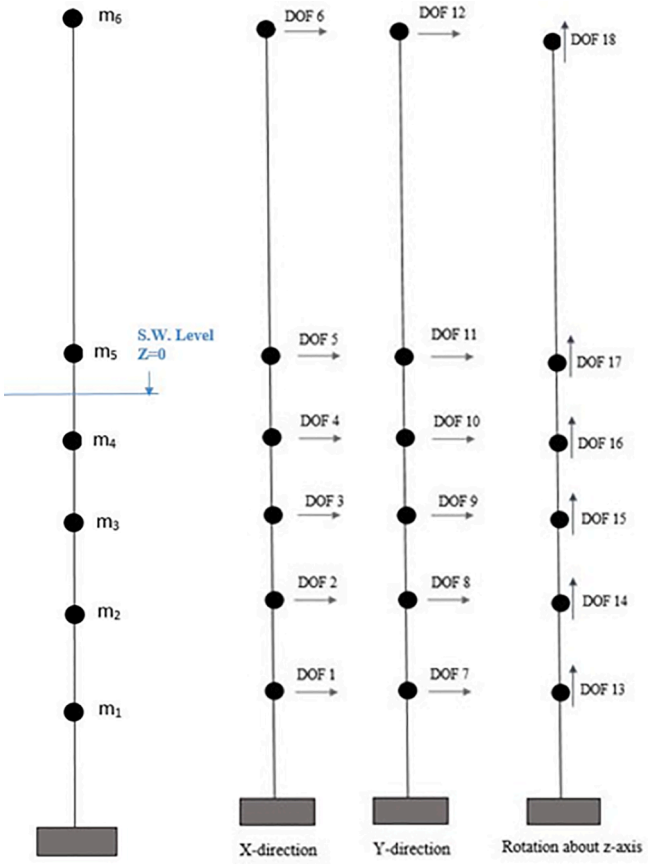

Fig. 1. Degrees of freedom for each lumped mass.

by Ziegler and Muskulus [12]. The fatigue resistance of welded connections made of high strength steel is also one important topic since most offshore structures rely on these connections to maintain structural integrity. Structural components with different scales normally show different fatigue behaviors, which can be virtually dominated by defects originated from multiple sources, including manufacturing processes [13]. The load ratio R, reflecting mean stress effects, will be changed with crack extension in the steel structures with complicated geometry [14]. The mean stress a welded joint may see in application, can be altered due to the welding processes implementing residual stresses

Table 2
Stiffness matrix values different for both wind turbines.

	HAWT	VAWT
$K_{5_x5_x}$	555651302 N/m	552709812 N/m
$K_{5_x6_x}$	−11657000 N/m	−8715500 N/m
$K_{6_x6_x}$	-$K_{5_x6_x}$	-$K_{5_x6_x}$
$K_{5_y5_y}$	394039445 N/m	391097956 N/m
$K_{5_y6_y}$	−11657000 N/m	−8715500 N/m
$K_{6_y6_y}$	$-K_{5_y6_y}$	$-K_{5_y6_y}$
$K_{5_\theta5_\theta}$	22340000000 N/rad	21110000000 N/rad
$K_{5_\theta6_\theta}$	−5123100000 N/rad	−3890500000 N/rad
$K_{6_\theta6_\theta}$	$-K_{5_\theta6_\theta}$	$-K_{5_\theta6_\theta}$

Table 3
Stiffness matrix values similar for both wind turbines.

$K_{1_x1_x}$	1295700000 N/m	$K_{4_x4_\theta}$	−1013.60 N/rad	$K_{3_y2_\theta}$	602.57 N/rad
$K_{1_x2_x}$	−570867389 N/m	$K_{4_x5_\theta}$	518.79 N/rad	$K_{3_y4_\theta}$	741.80 N/rad
$K_{2_x2_x}$	1010900000 N/m	$K_{5_x5_\theta}$	$-K_{4_x5_\theta}$	$K_{4_y4_\theta}$	-1471.1 N/rad
$K_{2_x3_x}$	−439982996 N/m	$K_{1_y1_y}$	918270000 N/m	$K_{4_y5_\theta}$	729.34 N/rad
$K_{3_x3_x}$	958857085 N/m	$K_{1_y2_y}$	−372688355 N/m	$K_{5_y5_\theta}$	$-K_{4_y5_\theta}$
$K_{3_x4_x}$	−518874089 N/m	$K_{2_y2_y}$	688606171 N/m	$K_{1_\theta1_\theta}$	229300000000 N/rad
$K_{4_x4_x}$	1062900000 N/m	$K_{2_y3_y}$	−315917816 N/m	$K_{1_\theta2_\theta}$	-73460000000 N/rad
$K_{4_x5_x}$	−543994304 N/m	$K_{3_y3_y}$	704835263 N/m	$K_{2_\theta2_\theta}$	111400000000 N/rad
$K_{5_x5_y}$	0 N/m	$K_{3_y4_y}$	−388917447 N/m	$K_{2_\theta3_\theta}$	-37940000000 N/rad
$K_{1_x1_\theta}$	−1100.5 N/rad	$K_{4_y4_y}$	771299895 N/m	$K_{3_\theta3_\theta}$	66620000000 N/rad
$K_{1_x2_\theta}$	544.42 N/rad	$K_{4_y5_y}$	−382382448 N/m	$K_{3_\theta4_\theta}$	-28680000000 N/rad
$K_{2_x2_\theta}$	−964.02 N/rad	$K_{1_y1_\theta}$	−1491 N/rad	$K_{4_\theta4_\theta}$	45900000000 N/rad
$K_{3_x2_\theta}$	419.60 N/rad	$K_{1_y2_\theta}$	710.85 N/rad	$K_{4_\theta5_\theta}$	-17220000000 N/rad
$K_{3_x4_\theta}$	494.84 N/rad	$K_{2_y2_\theta}$	−1313.40 N/rad		

[15], changing fatigue life and plotting S-N laboratory testing results. Uncertainties such as material variability, load variation or geometrical uncertainty influence the mechanical response of turbine bladed disks and are critical for the fatigue assessment and reliability evaluation because these disks operate under complex loadings from multiple sources [16] [17] [18] [19].

Various structural optimization studies have also been performed. Muskulus and Schafhirt [20] presented optimized approaches for structural optimization of wind turbines. Oest et al. [21] developed a method for optimization of a support structure for offshore wind turbines. In another study, Schafhirt et al. [22] used computer-aided optimization of OWTs for analysis of jacket support structures using a genetic algorithm, while Yoshida [23] used the same algorithm to present an optimized method for wind turbine towers. Lozano-Minguez et al. [24] presented a method to select a configuration for offshore wind turbine support structures. While the short-term response analysis of such jacket support structures for wind turbines was the subject of a study by Saha et al. [25], the scope of the present study is to find new uses for existing offshore infrastructure once it nears the end of its operational life or when the underground resource is depleted, allowing for an offshore-arena energy transition [26] [27].

The present work is a complementary study to that by Mendes et al. [28] where the possibility of repurposing an oil and gas platform was investigated and it was concluded that retrofitting should be done in order to extend the platform service life. Several authors have offered

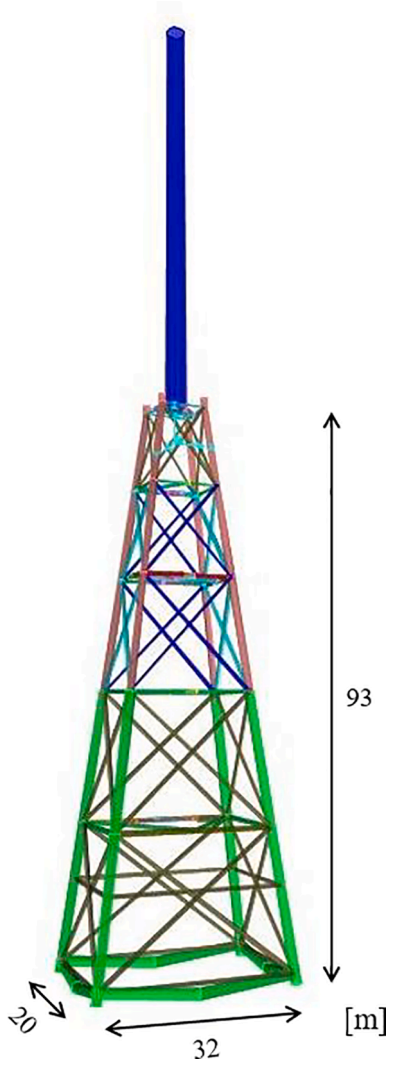

Fig. 2. Crown pile design detail.

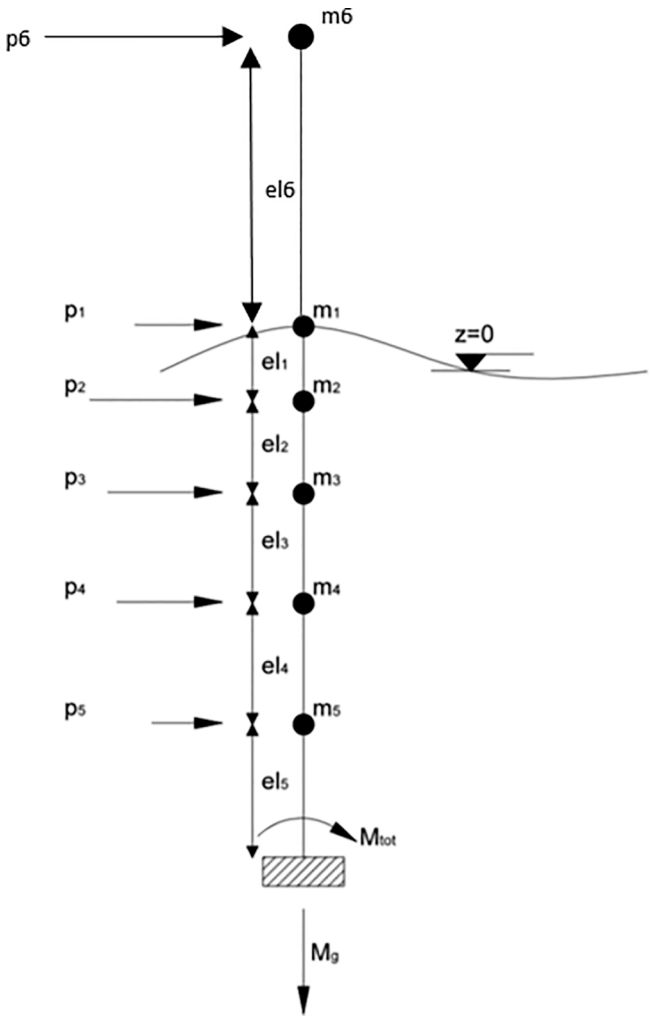

Fig. 3. Pile stress analysis of the model – Lumped mass labels.

different retrofitting solutions in order to reduce the cost for maintenance and increase reliability of the offshore structures. Schaver et al. [29] proposed a retrofit solution using bolted connections for in-service offshore wind turbines (OWTs) with monopile foundations using a finite element analysis-based optimization approach. Skavas et al. [30] discussed provisions in the DNVGL-RP-B401 standard used as a design code for cathodic protection (CP) in relation to new field experience and laboratory test data. This new knowledge may be employed to reduce the intrinsic conservatism in certain design parameters while still maintaining an intentional overcapacity to ensure that the CP system will allow the structure to achieve its design life. Seo et al. [31] analyzed a retrofit solution that involves drilling holes through the transition piece, grout, and monopile and installing pins, which would completely prevent vertical movement between the transition piece and monopile. Delwiche and Tavares [32] investigated the installation of aluminum anode strings inside a sealed internal section of the wind turbine monopiles as a retrofitting strategy. In the present study, the structure under investigation is an offshore jacket structure used for oil and gas purposes which has been adapted with a wind turbine placed on the top located in the Northern Adriatic Sea. This adaptation was the subject of

Table 4
Different values for the mass matrix for the 18-DOF model with the crown pile solution.

	VAWT & HAWT
$m_{5x} = m_{5y}$	1164000 kg
$m_{6x} = m_{6y}$	856840 kg
J_5	3774900 m^4
J_6	1659400 m^4

Table 5
Different values for the stiffness matrix for the 18-DOF model with the crown pile solution.

	VAWT & HAWT
K_{1x1x}	1303100000 N/m
K_{1y1y}	925070000 N/m
$K_{1\theta1\theta}$	230800000000 N/rad

Table 6
Maximum displacements in MATLAB and SAP2000 for both wind turbines with the crown pile solution.

	VAWT			HAWT		
Max displacements [m]	MATLAB	SAP	Error	MATLAB	SAP	Error
u_1	0.00684	0.00681	0.33%	0.00671	0.00671	0.03%
u_2	0.01533	0.01528	0.33%	0.01504	0.01504	0.01%
u_3	0.02581	0.02573	0.31%	0.02531	0.02531	−0.03%
u_4	0.03393	0.03383	0.29%	0.03324	0.03327	−0.08%
u_5	0.04055	0.04038	0.44%	0.03973	0.03967	0.15%
u_6	0.41000	0.40786	0.50%	0.308	0.30763	0.15%

Table 7
Extreme displacement limit values for horizontal- and vertical-axis wind turbines, in meters.

	HAWT	VAWT
$3\sigma(\xi_1)$	0.02220	0.02287
$3\sigma(\xi_2)$	0.04564	0.04742
$3\sigma(\xi_3)$	0.07279	0.07600
$3\sigma(\xi_4)$	0.09435	0.09843
$3\sigma(\xi_5)$	0.11393	0.11829
$3\sigma(\xi_6)$	0.14900	0.14400

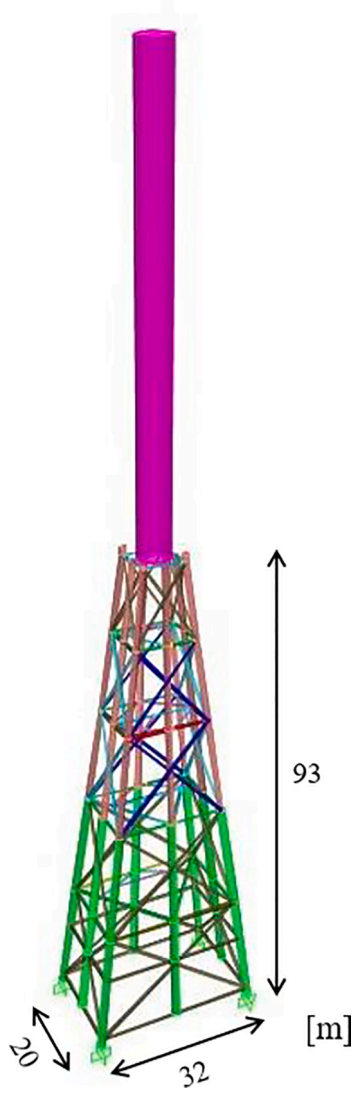

Fig. 5. Long pile 3D model in SAP2000.

Table 8
Horizontal- and vertical-axis turbine mass matrices results with the long pile solution.

	HAWT	VAWT
$m_{1x} = m_{1y}$	391996.52 kg	391996.52 kg
$m_{2x} = m_{2y}$	297389.07 kg	297389.07 kg
$m_{3x} = m_{3y}$	231431.99 kg	231431.99 kg
$m_{4x} = m_{4y}$	210552.69 kg	210552.69 kg
$m_{5x} = m_{5y}$	1205313.53 kg	984942.33 kg
$m_{6x} = m_{6y}$	856843.20 kg	710705 kg
J_1	82794850.81 m^4	82794850.81 m^4
J_2	35423174.52 m^4	35423174.52 m^4
J_3	17286727.97 m^4	17286727.97 m^4
J_4	9612815.30 m^4	9612815.30 m^4
J_5	4436258.91 m^4	3235073.77 m^4
J_6	1659377.20 m^4	3970550.49 m^4

Table 9
Undamped natural structural frequencies for free vibration for the horizontal- and vertical-axis wind turbines, in rad/s, with the long pile solution.

	HAWT	VAWT
ω_1	97.1673	3.3270
ω_2	98.4979	3.3826
ω_3	79.5425	9.0565
ω_4	78.7472	10.6572
ω_5	81.5854	20.3610
ω_6	58.4253	29.7847
ω_7	67.3602	31.3790
ω_8	65.4398	35.0275
ω_9	34.5305	46.7995
ω_{10}	53.6715	49.3028
ω_{11}	49.0355	58.7612
ω_{12}	40.2836	65.5182
ω_{13}	9.9807	66.1137
ω_{14}	21.8991	79.3726
ω_{15}	29.3539	79.6456
ω_{16}	3.5178	81.7001
ω_{17}	8.5352	97.3049
ω_{18}	3.4380	104.0179

prior work [28]; and in the present work, various solutions are presented and investigated. The authors are aware of the complexity of this problem. As such, the present study is limited, but in agreement with the assumptions made in prior work [28].

2. Theoretical overview

The set of equations representing structural motion in general can be written in the following matrix form:

Table 10
Damped natural frequencies with the corresponding damping ratios for both wind turbines with the long pile solution.

VAWT		HAWT	
ζ_i	ω_d (rad/s)	ζ_i	ω_d (rad/s)
0.0500	3.3228	0.0500	97.0457
0.0500	3.3784	0.0500	98.3747
0.0767	9.0298	0.0711	79.4387
0.0873	10.6165	0.0791	78.6440
0.1558	20.1122	0.1740	81.4800
0.2248	29.0226	0.2483	58.3310
0.2365	30.4888	0.2904	67.2636
0.2634	33.7904	0.3041	65.3440
0.3505	43.8299	0.4061	34.4208
0.3691	45.8214	0.4066	53.5771
0.4393	52.7870	0.4805	48.9399
0.4895	57.1312	0.5227	40.1819
0.4940	57.4852	0.5554	9.6699
0.5925	63.9376	0.6250	21.7480
0.5946	64.0383	0.6685	29.2326
0.6099	64.7482	0.7071	2.5255
0.7260	66.9179	0.7631	8.1717
0.7760	65.6137	0.8272	2.4132

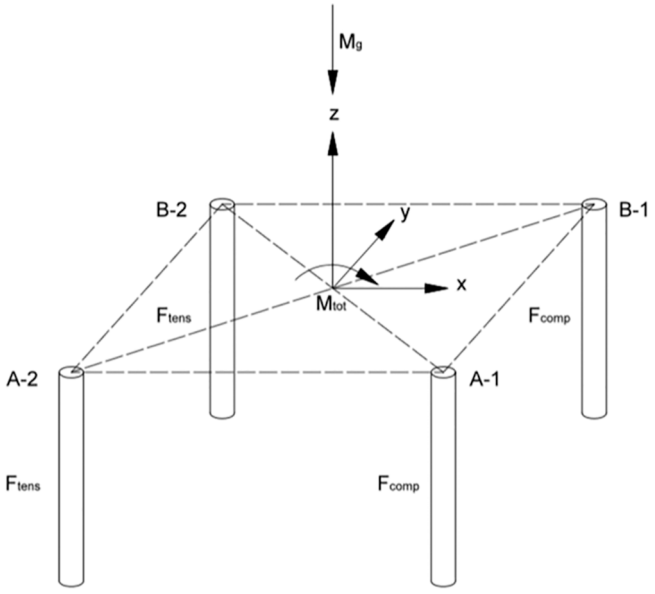

Fig. 4. Pile stress analysis of the model – Pile capacity.

$$\mathbf{M}\ddot{\boldsymbol{\xi}} + \mathbf{C}\dot{\boldsymbol{\xi}} + \mathbf{K}\boldsymbol{\xi} = \mathbf{p} \tag{1}$$

Where **M** represents the mass matrix, **C** represents the damping matrix and **K** represents the stiffness matrix. Eq. (1) represents a finite set of N ordinary, linear differential equations in N coordinates that describe the dominant characteristics of the structural motion. The degrees of freedom are collected in the vector $\boldsymbol{\xi}$:

$$\boldsymbol{\xi} = [\xi_1, \xi_2, \ldots, \xi_N]^T \tag{2}$$

The loading vector $\mathbf{p} = \mathbf{p}(t)$ is comprised of N loads $p_i, i = 1, 2, \ldots, N$ where the load $p_i = p_i(t)$ is in the direction of the coordinate, $\boldsymbol{\xi}$.

In this analysis, the mass matrix **M** is assumed to be a diagonal matrix with elements $m_i > 0, i = 1, 2, \ldots, N$, in which the element's subscript defines the inertia and rotary inertia in the direction of ξ_i.

Each generalized coordinate represents either a displacement or a rotation. The mass lumping method is most common for popular method of discretizing the supporting framework and the rigid body portions of

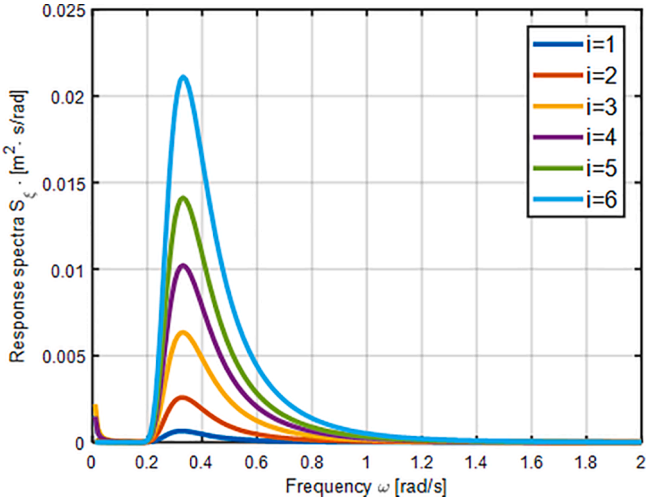

Fig. 6. Response spectra for the displacements in physical coordinates with the long pile configuration for the horizontal-axis wind turbine.

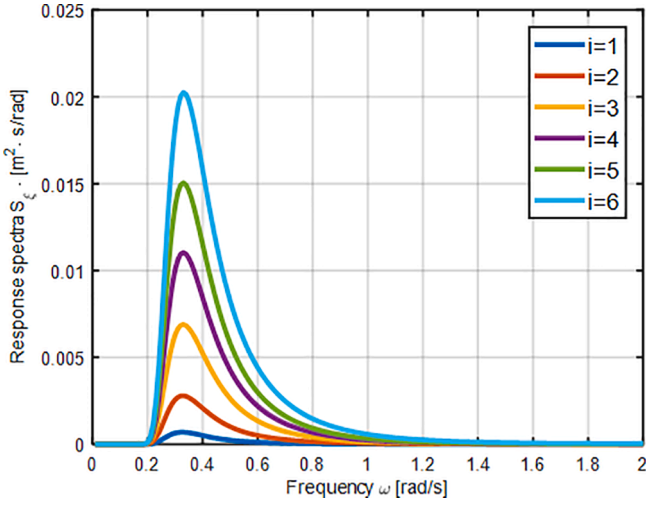

Fig. 7. Response spectra for the displacements in physical coordinates with the long pile configuration for the vertical-axis wind turbine.

Table 11
Maximum displacements in MATLAB and SAP2000 for both wind turbines with the long pile solution.

	VAWT			HAWT		
Max displacements [m]	MATLAB	SAP	Error	MATLAB	SAP	Error
u_1	0.00777	0.00775	0.31%	0.00752	0.00766	−1.77%
u_2	0.01635	0.01630	0.27%	0.01581	0.01611	−1.83%
u_3	0.02696	0.02689	0.26%	0.02605	0.02655	−1.87%
u_4	0.03464	0.03456	0.23%	0.03343	0.03410	−1.97%
u_5	0.04019	0.04003	0.38%	0.03871	0.03947	−1.91%
u_6	0.40962	0.40751	0.52%	0.30100	0.30700	−2.07%

Table 12
Extreme displacement limit values for horizontal- and vertical-axis wind turbines, in meters.

	HAWT	VAWT
$3\sigma(\xi_1)$	0.04051	0.03876
$3\sigma(\xi_2)$	0.07541	0.07836
$3\sigma(\xi_3)$	0.12096	0.12456
$3\sigma(\xi_4)$	0.15301	0.15807
$3\sigma(\xi_5)$	0.17904	0.18455
$3\sigma(\xi_6)$	0.221	0.219

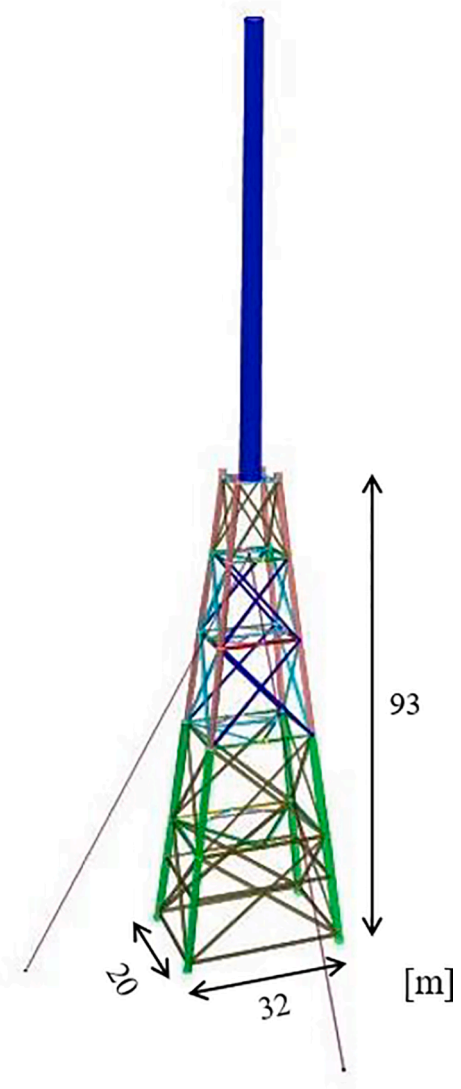

Fig. 8. Mooring line configuration in a 3D model in SAP2000.

the offshore structure. The stiffness matrix **K** for a N degree of freedom structure is a symmetric matrix of $N \times N$ elements. The stiffness constant k_{ij} is that force that is required in the direction of ξ_i to cause a unit elastic displacement $\xi_{sj} = 1$ while all displacements $\xi_{si} = 0$ for $i \neq j$. For a structure with N degrees of freedom, the damping matrix **C** is defined as a symmetric matrix of $N \times N$ constants, c_{ij}.

In physical systems, damping allows dissipation of energy stored

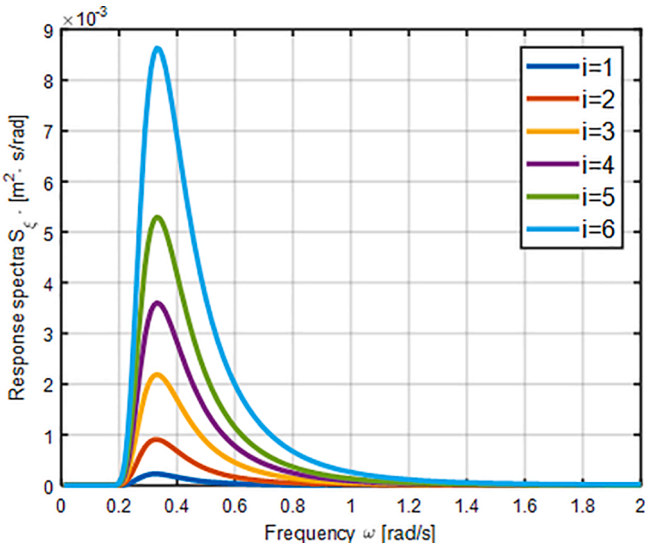

Fig. 9. Response spectra for the displacements in physical coordinates with the mooring lines solution for the horizontal-axis wind turbine.

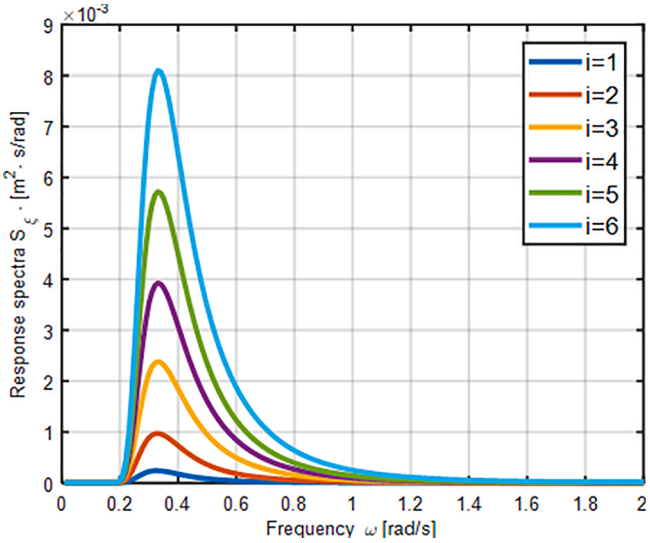

Fig. 10. Response spectra for the displacements in physical coordinates with the mooring lines solution for the vertical-axis wind turbine.

Table 13
Maximum displacements in MATLAB and SAP2000 for both wind turbines with the mooring lines solution, in meters.

	VAWT			HAWT		
Max displacements [m]	MATLAB	SAP	Error	MATLAB	SAP	Error
u_1	0.00671	0.00669	0.33%	0.00658	0.00766	−0.01%
u_2	0.01495	0.01490	0.33%	0.01466	0.01466	−0.01%
u_3	0.02511	0.02503	0.32%	0.02461	0.02462	−0.04%
u_4	0.03295	0.03286	0.30%	0.03228	0.03231	−0.10%
u_5	0.03957	0.03940	0.45%	0.03876	0.03871	0.14%
u_6	0.4090	0.4070	0.53%	0.30700	0.30700	0.14%

Table 14
Extreme displacement limit values for horizontal- and vertical-axis wind turbines.

	HAWT	VAWT
$3\sigma(\xi_1)$	0.02197	0.02260
$3\sigma(\xi_2)$	0.04471	0.04642
$3\sigma(\xi_3)$	0.07093	0.07402
$3\sigma(\xi_4)$	0.09173	0.09564
$3\sigma(\xi_5)$	0.11135	0.11552
$3\sigma(\xi_6)$	0.14400	0.14000

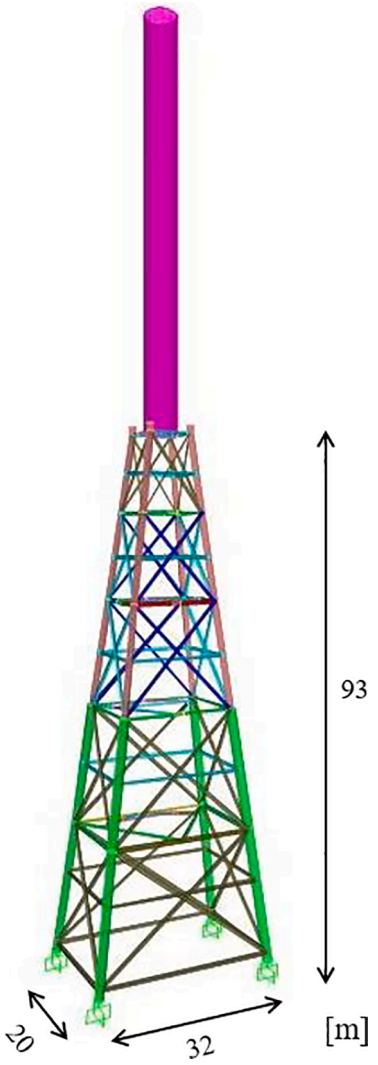

Fig. 11. Stirrups as part of 3D Model in SAP2000.

during oscillations. In this analysis, the damping force q_{Di} for the structural mode coordinate ξ, is assumed to be a linear combination of the generalized coordinate velocities $\dot{\xi}_i, i = 1, 2, \ldots, N$:

$$\mathbf{q}_D = \mathbf{C}\dot{\boldsymbol{\xi}} \tag{3}$$

The damping matrix can be cast in several different specialized forms, each of which has the advantage of easily utilizing available experimental data to determine the elements c_{ij}. One such form is Rayleigh damping in which **C** is proportional to the system's mass and stiffness:

$$\mathbf{C} = a_1\mathbf{K} + a_2\mathbf{M} \tag{4}$$

where a_1 and a_2 are Rayleigh constants, and they are chosen to match desired damping levels in any two modes of vibration. The normal mode method is used for the solution of the equations of motion. Rayleigh constants are determined using a standardized procedure [33]. All of the analysis steps necessary for the simplified design of an offshore structure is carried out by using a 10-step modeling approach:

1. Establishing the structural and environmental parameters
2. Definition of the free undamped motion of the structure
3. Determination of the damped frequencies of the structure
4. Response to environmental loads
5. Maximum load applied
6. Time-domain solution
7. Transfer function definition
8. Spectral density function estimaton of the response
9. Response spectrum
10. 3σ approach

This analysis approach is done according to Ref. [33] and for all retrofitting activities this procedure is repeated.

To calculate the masses the specific weight of steel 7850 kg/m^3 is considered and the structure is modeled in ETABS software. ETABS is capable of considering each horizontal level of the jacket as a story and estimates the total masses and moments of inertia of all elements surrounding the center of each horizontal level. The mass of a vertical-axis wind turbine results from the blades and tower and is uniformly distributed along the height. Hence the total mass is lumped at the center of mass which is located at the mid-height of the tower. Only the rotor mass is added to the base of tower which is the case for vertical-axis wind turbines. As for the horizontal-axis wind turbine, the mass is lumped at the top of the tower. The mass of the tower is assigned to the top and base of the tower by ETABS. Darrieus vertical-axis wind turbine and the upwind horizontal-axis wind turbine were the types of wind tower turbines chosen. It is important to note that the model has 3 degrees of freedom per level (and therefore the mass matrix **M** results of the 18-DOF model created in MATLAB for the vertical- and horizontal-axis turbines are presented in Table 1 and given by Eq. 5:

$$\mathbf{M} = \begin{bmatrix} \mathbf{M}_x & 0 & 0 \\ 0 & \mathbf{M}_y & 0 \\ 0 & 0 & \mathbf{J} \end{bmatrix} \tag{5}$$

for the horizontal and vertical axis wind turbines, where

$$\mathbf{M}_i = \mathrm{diag}(\, m_{1i} \quad m_{2i} \quad m_{3i} \quad m_{4i} \quad m_{5i} \quad m_{6i}\,) \quad \text{for} \quad i = x, y \tag{6}$$

$$\mathbf{J} = \mathrm{diag}(\, J_1 \quad J_2 \quad J_3 \quad J_4 \quad J_5 \quad J_6\,) \tag{7}$$

The stiffness matrix is determined corresponding to degrees of freedom in the x, y and θ direction. Fig. 1 presents the degrees of freedom considered in this structure. Based on SAP2000, the stiffness matrices K for the vertical- and horizontal-axis are:

$$K = \begin{bmatrix} \mathbf{K}_{xx} & \mathbf{K}_{xy} & \mathbf{K}_{x\theta} \\ \mathbf{K}_{xy}^{\top} & \mathbf{K}_{yy} & \mathbf{K}_{y\theta} \\ \mathbf{K}_{x\theta}^{\top} & \mathbf{K}_{y\theta}^{\top} & \mathbf{K}_{\theta\theta} \end{bmatrix} \tag{8}$$

where

$$\mathbf{K}_{xx} = \begin{bmatrix} K_{1_x1_x} & K_{1_x2_x} & 0 & 0 & 0 & 0 \\ & K_{2_x2_x} & K_{2_x3_x} & 0 & 0 & 0 \\ & & K_{3_x3_x} & K_{3_x4_x} & 0 & 0 \\ & & & K_{4_x4_x} & K_{4_x5_x} & 0 \\ & & & & K_{5_x5_x} & K_{5_x6_x} \\ \text{sym} & & & & & K_{6_x6_x} \end{bmatrix}, \mathbf{K}_{xy} = \begin{bmatrix} 0 & 0 & 0 & 0 & 0 & 0 \\ 0 & 0 & 0 & 0 & 0 & 0 \\ 0 & 0 & 0 & 0 & 0 & 0 \\ 0 & 0 & 0 & 0 & 0 & 0 \\ 0 & 0 & 0 & 0 & 0 & 0 \\ 0 & 0 & 0 & 0 & 0 & 0 \end{bmatrix}$$

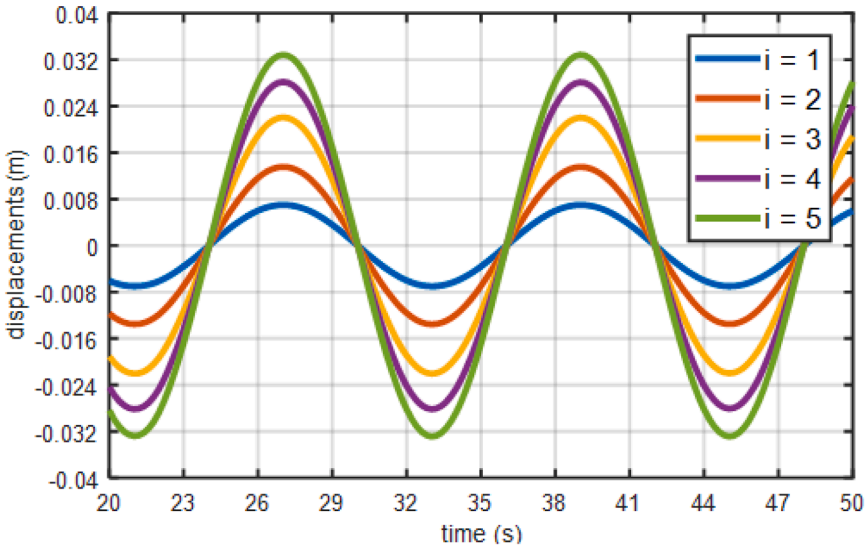

(a)

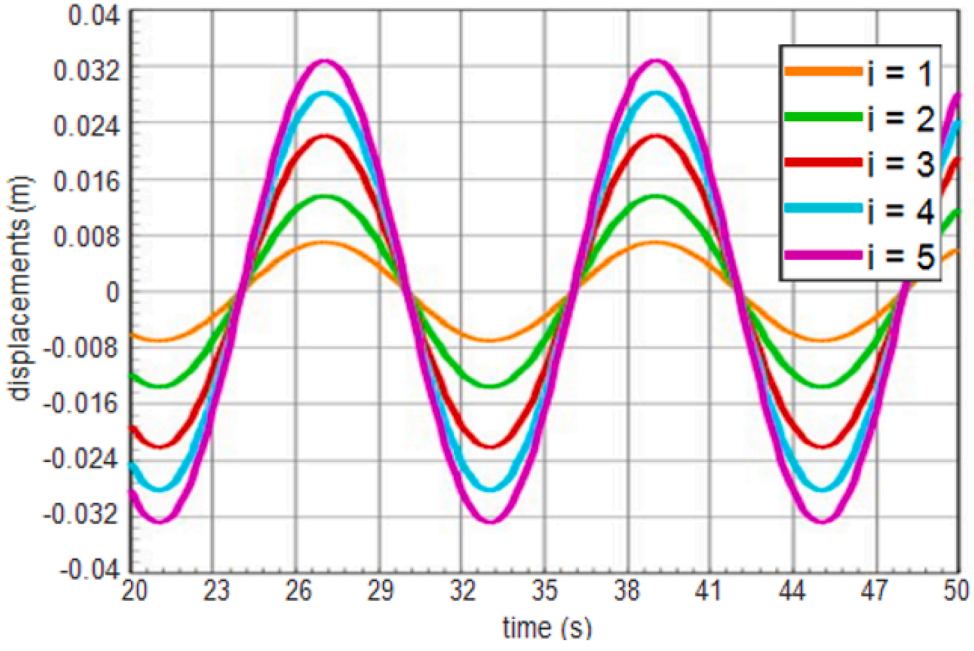

(b)

Fig. 12. Response to a harmonic wave and wind force in mass 1 to 5 for the horizontal-axis wind turbine in a) MATLAB and b) SAP2000.

Table 15
Horizontal- and vertical-axis turbine mass matrices results with the stirrups solution.

	HAWT	VAWT
$m_{1x} = m_{1y}$	285088.87 kg	285088.87 kg
$m_{2x} = m_{2y}$	174839.22 kg	174839.22 kg
$m_{3x} = m_{3y}$	141432.97 kg	141432.97 kg
$m_{4x} = m_{4y}$	131176.17 kg	131176.17 kg
$m_{5x} = m_{5y}$	1167249.76 kg	946878.56 kg
$m_{6x} = m_{6y}$	856843.20 kg	710705 kg
J_1	70231947.29 m^4	70231947.29 m^4
J_2	26708363.72 m^4	26708363.72 m^4
J_3	13394269.55 m^4	13394269.55 m^4
J_4	7531893.70 m^4	7054173.79 m^4
J_5	226030.29 m^4	2718716.90 m^4
J_6	1659377.20 m^4	3970550.49 m^4

Table 16
Undamped natural structural frequencies for free vibration for the horizontal- and vertical-axis wind turbines, in rad/s, with the stirrups mechanism.

	HAWT	VAWT
ω_1	3.4655	3.3453
ω_2	3.5209	3.3841
ω_3	9.3117	9.9956
ω_4	10.5096	11.3355
ω_5	26.4639	22.8663
ω_6	36.3415	32.7214
ω_7	41.5385	36.7214
ω_8	45.0566	41.9610
ω_{18}	58.3230	52.2057
ω_9	61.9605	62.2413
ω_{10}	71.1788	71.4972
ω_{11}	82.5881	80.2325
ω_{12}	87.1638	87.2576
ω_{13}	100.8372	99.2818
ω_{14}	101.8382	100.9437
ω_{15}	111.4613	111.5673
ω_{16}	125.7292	125.8474
ω_{17}	137.7759	129.3486

$$\mathbf{K}_{x\theta} = \begin{bmatrix} K_{1_x1_\theta} & K_{1_x2_\theta} & 0 & 0 & 0 & 0 \\ K_{2_x1_\theta} & K_{2_x2_\theta} & 0 & 0 & 0 & 0 \\ 0 & K_{3_x2_\theta} & 0 & K_{3_x4_\theta} & 0 & 0 \\ 0 & 0 & 0 & K_{4_x4_\theta} & K_{4_x5_\theta} & 0 \\ 0 & 0 & 0 & K_{5_x4_\theta} & K_{5_x5_\theta} & 0 \\ 0 & 0 & 0 & 0 & 0 & 0 \end{bmatrix}, \quad \mathbf{K}_{yy} = \begin{bmatrix} K_{1_y1_y} & K_{1_y2_y} & 0 & 0 & 0 & 0 \\ & K_{2_y2_y} & K_{2_y3_y} & 0 & 0 & 0 \\ & & K_{3_y3_y} & K_{3_y4_y} & 0 & 0 \\ & & & K_{4_y4_y} & K_{4_y5_y} & 0 \\ & & & & K_{5_y5_y} & K_{5_y6_y} \\ \text{sym} & & & & & K_{6_y6_y} \end{bmatrix}$$

$$\mathbf{K}_{y\theta} = \begin{bmatrix} K_{1_y1_\theta} & K_{1_y2_\theta} & 0 & 0 & 0 & 0 \\ K_{2_y1_\theta} & K_{2_y2_\theta} & 0 & 0 & 0 & 0 \\ 0 & K_{3_y2_\theta} & 0 & K_{3_y4_\theta} & 0 & 0 \\ 0 & 0 & 0 & K_{4_y4_\theta} & K_{4_y5_\theta} & 0 \\ 0 & 0 & 0 & K_{5_y4_\theta} & K_{5_y5_\theta} & 0 \\ 0 & 0 & 0 & 0 & 0 & 0 \end{bmatrix}, \quad \mathbf{K}_{\theta\theta} = \begin{bmatrix} K_{1_\theta1_\theta} & K_{1_\theta2_\theta} & 0 & 0 & 0 & 0 \\ & K_{2_\theta2_\theta} & K_{2_\theta3_\theta} & 0 & 0 & 0 \\ & & K_{3_\theta3_\theta} & K_{3_\theta4_\theta} & 0 & 0 \\ & & & K_{4_\theta4_\theta} & K_{4_\theta5_\theta} & 0 \\ & & & & K_{5_\theta5_\theta} & K_{5_\theta6_\theta} \\ \text{sym} & & & & & K_{6_\theta6_\theta} \end{bmatrix}$$

In Table 2 are presented the stiffness values that are different for both wind turbines without any retrofitting solution.

In Table 3 are presented the stiffness values that are similar for both wind turbines without any retrofitting solution.

3. Retrofitting activities

This research is based on a previous study [28] where the structural behaviour of two different wind turbines was investigated. Mendes et al. [28] concluded that the jacket platform was not safe when including the wind turbines. Therefore, retrofitting solutions should be proposed in order to strengthen the structure so that environmental actions can absorbed by the system safely. Retrofitting consists in making changes to an existing structure to protect it, reducing the vulnerability to damage of the existing structure, by increasing the strength and thus the overall lifespan of the structure.

The structural configuration under study is the same jacket with a wind turbine tower installed on top. In this work, MATLAB and SAP2000 are used in the analyses. The main objective of this research is to look for a suitable intervention which ensures that the modified offshore structure will behave safely. Five retrofitting activities that can be employed for the offshore wind turbine are proposed:

Table 17
The damped frequencies with the corresponding damping factors for both wind turbines with the stirrups solution.

VAWT		HAWT	
ζ_i	ω_d (rad/s)	ζ_i	ω_d (rad/s)
0.0500	3.3411	0.0500	3.4612
0.0500	3.3798	0.0500	3.5165
0.0827	9.9614	0.0760	9.2847
0.0916	11.2878	0.0835	10.4729
0.1736	22.5192	0.1927	25.9679
0.2525	32.5611	0.2625	35.0672
0.2751	35.3042	0.2994	39.6333
0.3138	39.8418	0.3244	42.6200
0.3895	48.0827	0.4189	52.9593
0.4638	55.1417	0.4448	55.4924
0.5324	60.5215	0.5106	61.1995
0.5972	64.3548	0.5921	66.5538
0.6493	66.3624	0.6248	68.0556
0.7385	66.9388	0.7225	69.7129
0.7509	66.6699	0.7297	69.6354
0.8297	62.2761	0.7985	67.1022
0.9357	44.3892	0.9005	54.6737
0.8617	35.4440	0.9867	22.4329

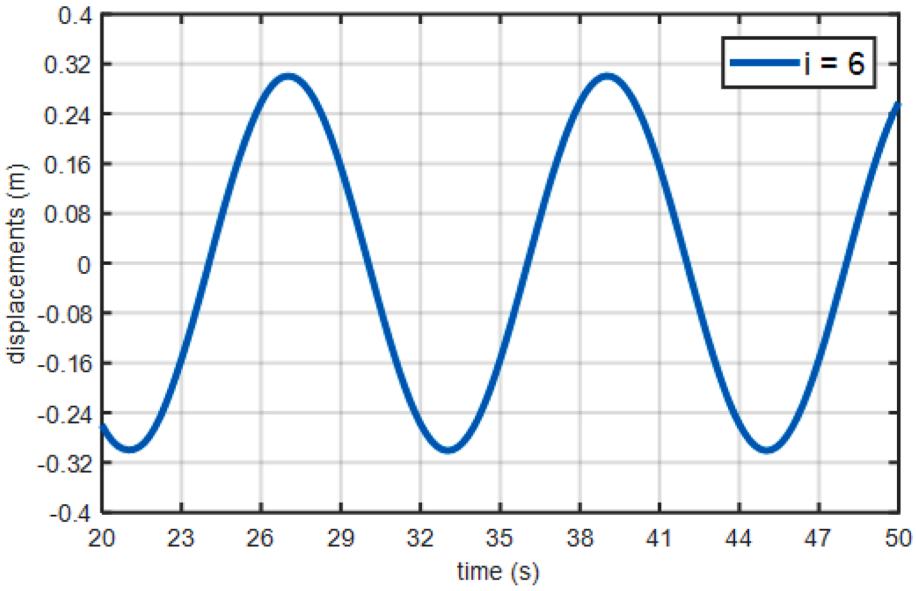

(a)

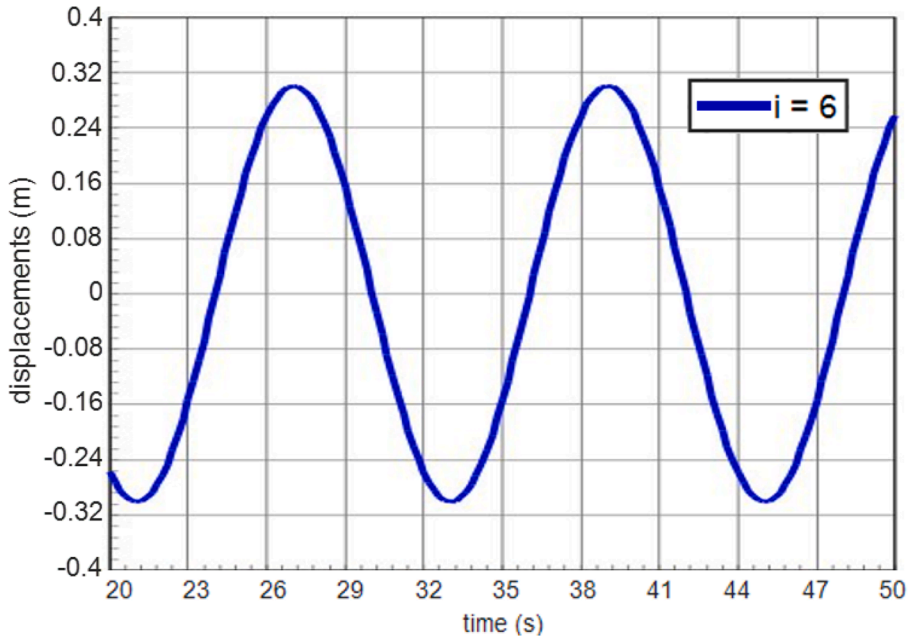

(b)

Fig. 13. Response to harmonic wave and wind force for mass 6 for the horizontal-axis wind turbine in a) MATLAB and b) SAP2000.

- Four of the five solutions are focused on intervention methods related to the substructure and consider the same wind turbine tower.

1. Crown pile – In addition to the four corner piles, extra four piles are placed at the midspan of each side at $z = -d$ connected each to the other piles with a rectangular ring;
2. Long pile – Four extra legs positioned from top to bottom in each side of the jacket connecting each horizontal plane are added to the model;
3. Mooring lines – A mooring line system that links the forth horizontal plane of the jacket to the seabed in both x- and y-direction causing restrictions to structure movement;
4. Stirrups – Each side of the jacket has been added with four extra horizontal stirrups;

- The fifth method is related to the superstructure.

1. 2 MW wind turbine - Replacing the study with a 2 MW horizontal- and vertical-axis wind turbine instead of 5 MW horizontal- and vertical-axis wind turbine;

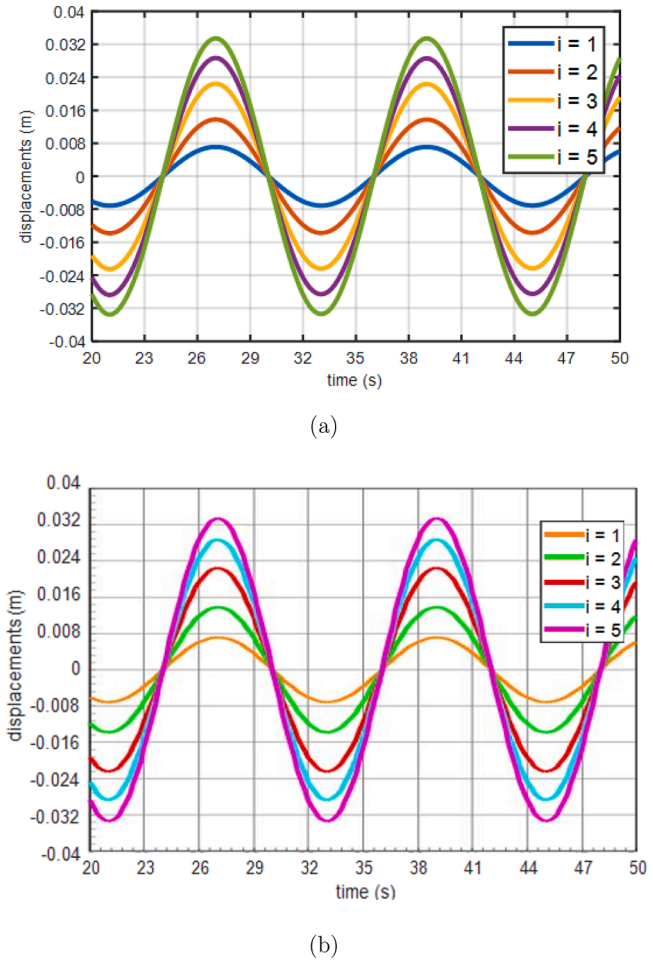

Fig. 14. Response to a harmonic wave and wind force in mass 1 to 5 for the vertical-axis wind turbine in a) MATLAB and b) SAP2000.

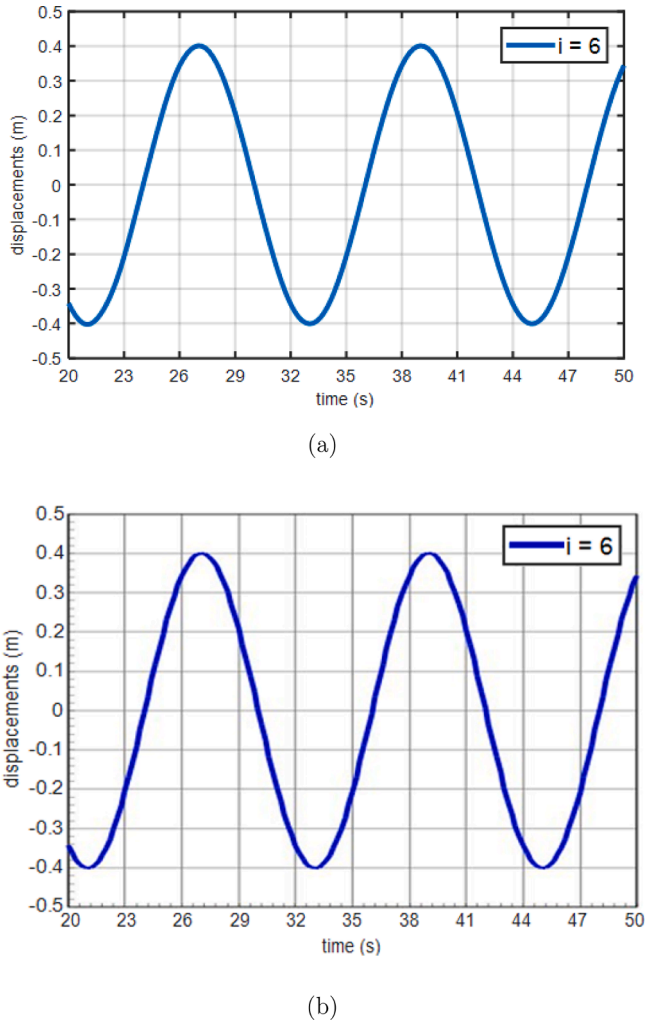

Fig. 15. Response to harmonic wave and wind force for mass 6 for the vertical-axis wind turbine in a) MATLAB and b) SAP2000.

3.1. Crown pile

All analysis steps necessary for the simplified design of an offshore structure have been done using a 10-step modeling approach and are represented in Mendes et al. [28]. Therefore when introducing a new retrofitting solution, all analysis steps should be repeated. The crown pile solution introduces the same configuration of the 18DOF model with four extra piles at the base of the jacket placed at the midspan of each side at $z = -d$ and connected to the main piles with a rectangular ring. The models are considered with the z axis pointing upward with the sea bottom at $z = -d$. Fig. 2,3, shows the new configuration with the crown pile solution:

The model that represents the crown pile configuration is like the 18-DOF model referenced in Mendes et al. [28] for the vertical- and horizontal-axis wind turbines with some differences in the mass and stiffness matrices M and K. Tables 4 and 5 present the different mass and stiffness values with the crown pile solution for the 18-DOF model.

For the undamped and damped natural frequencies, the values are practically the same varying around 0.01–0.1 rad/s from the original 18-DOF model without the crown pile solution. The damped frequencies factors are also almost the same with differences of around 0.0001–0.001 Hz for both wind turbines types.

The Airy wave theory is applied, according to Wilson and Muga [33], and the motion of the structure is much smaller than the motion of the wave and therefore the Morison's equation can be used. The inertia term of the hydrodynamic force is represented by the inertia coefficient $C_M = 2$ and the drag term by the drag coefficient $C_D = 0.8$. The structure has been modeled with four vertical legs plus two horizontal cross braces, which are normal to the flow. The calculation of the wave forces follows the guidelines reported by classical books on offshore structural modeling [33]. Wave loads for the problem under consideration, in kN, are:

$p_1 = 158110$; $p_2 = 230970$; $p_3 = 393210$; $p_4 = 646840$; $p_5 = 345450$;

For level 6 corresponding to the wind loads, the forces are different for each wind turbine. The p_6 force is 3055000 kN and 3127100 kN for the horizontal- and vertical-axis turbine, respectively.

Considering the wind force applied on the wind turbine with the wave load which was already determined, the maximum compression force in the piles is obtained in B_1 and it is equal to $F_{B1} = -10416$ kN and $F_{B1} = -10104$ kN for the horizontal- and vertical-axis wind turbine, respectively. It is possible to conclude that the compression loads are lower than the pile compression limit so this configuration helps the wind turbine to work in terms of stability.

The maximum displacements obtained with MATLAB and SAP2000 are of the same magnitude. Table 6 presents the maximum displacements for the horizontal- and vertical-axis wind turbine with the crown pile solution.

As is clear, there is consistency between the two procedures so the defined models are assumed to be appropriate. The response to harmonic wave and wind forces for mass 1 to 6 in MATLAB and SAP2000 are practically the same as in the 18-DOF model.

The last step necessary for the simplified design of an offshore

Table 18
Maximum displacements in MATLAB and SAP2000 for both wind turbines with the stirrups solution.

	VAWT			HAWT		
Max displacements	MATLAB	SAP	Error	MATLAB	SAP	Error
u_1	0.00715	0.007122	0.35%	0.00701	0.00701	−0.06%
u_2	0.01383	0.013786	0.31%	0.01356	0.01358	−0.12%
u_3	0.02254	0.022475	0.28%	0.02208	0.02212	−0.18%
u_4	0.02881	0.028732	0.26%	0.02820	0.02826	−0.24%
u_5	0.03357	0.033423	0.43%	0.03288	0.03285	0.08%
u_6	0.403	0.400747	0.54%	0.30100	0.30100	0.08%

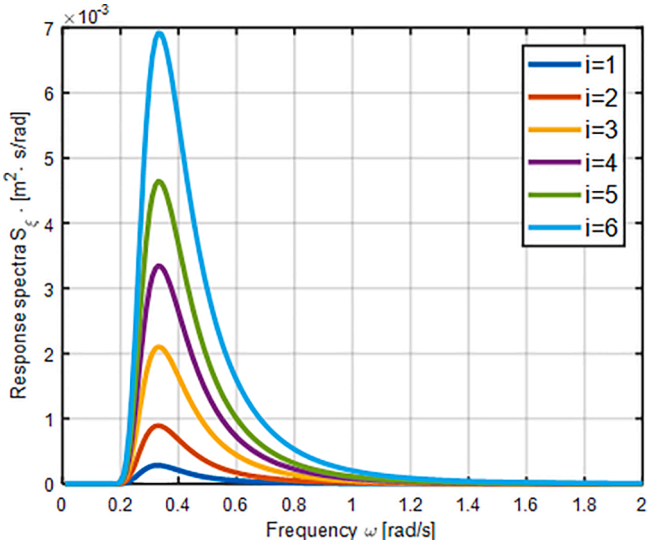

Fig. 16. Response spectra for the displacements in physical coordinates with the stirrups elements for the horizontal-axis wind turbine.

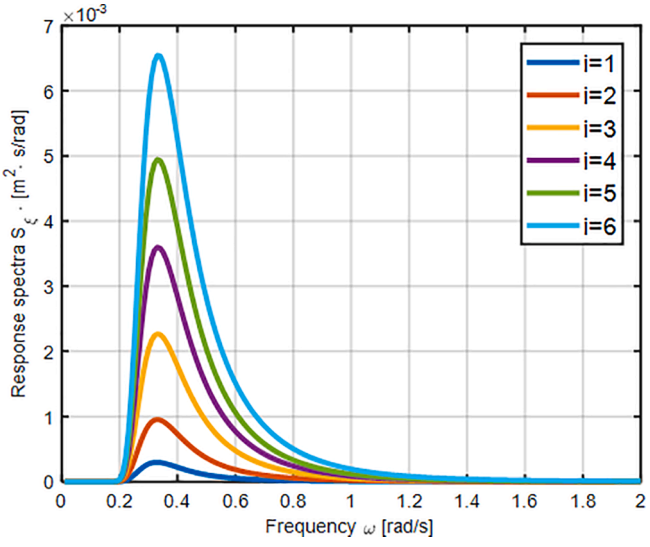

Fig. 17. Response spectra for the displacements in physical coordinates with the stirrups elements for the vertical-axis wind turbine.

structure includes the stochastic approach design using the 3σ approach. This verification is needed to check if the structure is safe or not. By computing the area covered by the response displacement power spectra, the variance of such displacements $\sigma^2(\xi_k)$ can be computed. The extreme limits of ξ_k are $\pm 3\sigma(\xi_k)$ for $k = 1, 2, \ldots, 5$. If the static stresses and the deflections of the members are within these extreme limit

Table 19
Extreme displacement limit values for horizontal- and vertical-axis wind turbines with the stirrups solution.

	HAWT	VAWT
$3\sigma(\xi_1)$	0.02472	0.02544
$3\sigma(\xi_2)$	0.04467	0.04626
$3\sigma(\xi_3)$	0.06967	0.07234
$3\sigma(\xi_4)$	0.08830	0.09148
$3\sigma(\xi_5)$	0.10406	0.10727
$3\sigma(\xi_6)$	0.12900	0.12600

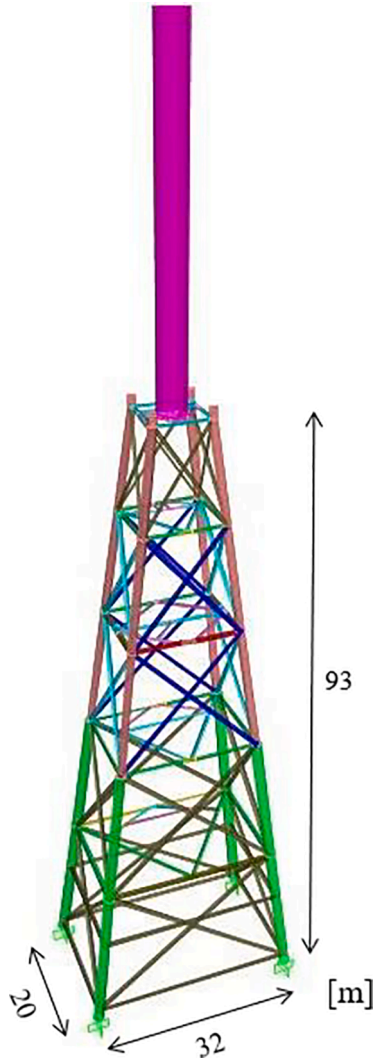

Fig. 18. 2 MW turbine as part of 3D Model in SAP2000.

Table 20
Horizontal- and vertical-axis turbine mass matrices results with the 2 MW wind turbines

	HAWT	VAWT
$m_{1x} = m_{1y}$	278263.09 kg	278263.09 kg
$m_{2x} = m_{2y}$	162534.86 kg	162534.86 kg
$m_{3x} = m_{3y}$	131654.74 kg	131654.74 kg
$m_{4x} = m_{4y}$	123604.06 kg	123604.06 kg
$m_{5x} = m_{5y}$	1037266.5 kg	743583.40 kg
$m_{6x} = m_{6y}$	460132.40 kg	279541.70 kg
J_1	68867970.64 m^4	68867970.64 m^4
J_2	24647179.72 m^4	24647179.72 m^4
J_3	12364431.90 m^4	12364431.90 m^4
J_4	7054173.79 m^4	7054173.79 m^4
J_5	3360144.52 m^4	2232113.41 m^4
J_6	1244642.62 m^4	583125.19 m^4

Table 21
Stiffness matrix values different for both wind turbine types with a 2 MW wind turbine solution.

	HAWT	VAWT
$K_{5_\theta 5_\theta}$	24050000000 N/rad	18980000000 N/rad
$K_{5_\theta 6_\theta}$	−6830800000 N/rad	−1760600000 N/rad
$K_{6_\theta 6_\theta}$	$-K_{5_\theta 6_\theta}$	$-K_{5_\theta 6_\theta}$

Table 22
Undamped natural structural frequencies for free vibration for the horizontal- and vertical-axis wind turbines, in rad/s, for the 2 MW wind turbine.

	HAWT	VAWT
ω_1	5.8436	5.9012
ω_2	6.3931	6.1529
ω_3	10.6126	10.4112
ω_4	11.5013	11.8403
ω_5	24.0237	25.1652
ω_6	33.8569	34.4592
ω_7	39.6912	40.3705
ω_8	43.5194	44.9896
ω_9	55.6089	55.1327
ω_{10}	60.5958	55.9503
ω_{11}	65.8271	66.2647
ω_{12}	76.0985	71.3138
ω_{13}	76.6512	76.2381
ω_{14}	91.3246	88.2748
ω_{15}	91.6646	91.8355
ω_{16}	96.9968	97.1183
ω_{17}	109.6871	112.6564
ω_{18}	113.5062	113.6543

values, then the structure is assumed safe. Assuming a Gaussian process, there is only a 0.26 % chance that each response falls outside the $\pm 3\sigma(\xi_k)$ limits. The extreme displacement limit values for horizontal- and vertical-axis wind turbines, in meters, are:

It possible to conclude that the structure is not safe at the node 6 which is at the top of the wind turbine tower for both wind turbines since the limits presented in Table 7 are lower than the max displacements for node 6 presented in Table 6.

3.2. Long pile

The long pile solution involves the introduction of four extra legs positioned from top to bottom on each side of the jacket linking each horizontal plane. The geometry of the extra legs is the same as the corner legs. The extra leg diameter varies from 1200 mm by 40 mm at the top levels to 1600 mm by 50 mm at the bottom levels. Fig. 5 displays the model with the long pile solution.

The long pile lumped masses are calculated according to the same approach along with the four extra legs. In this case, the mass matrix changes completely (see Table 8).

As for the stiffness matrix K it changes a lot and stiffness values are larger compared to the previous models due to the added legs.

The eighteen undamped natural structural frequencies from free vibration analysis for the horizontal- and vertical-axis wind turbines with the long pile solution, given in rad/s, are presented in Table 9;these frequencies are significantly different from the 18-DOF model without the long pile solution. Table 10 lists the damped frequencies with the corresponding damping factors for the horizontal- and vertical-axis wind turbines for the long pile solution.

The structure is modelled with eight vertical legs, so $N_l = 8$ and two horizontal cross braces $N_c = 2$ which are normal to the flow. As a result, the calculation of the wave forces following the guidelines reported by classical books of offshore structures [33], leads to different values which are, in kN:

$p_1 =$ 158110; $p_2 =$ 230970; $p_3 =$ 687470; $p_4 =$ 1141600; $p_5 =$ 690810;

The forces applied at the top node of the model p_6 (wind load) are 3055000 kN and 3127100 kN for the horizontal- and vertical-axis turbine, respectively, as cited before.

Considering the same wind force applied on the wind turbine with the wave load which already determined before and the configuration from Fig. 4, the maximum compression force in the piles is obtained in B_1 and it is equal to $F_{B1} = -20012$ kN and $F_{B1} = -19320$ kN for the horizontal- and vertical-axis wind turbine, respectively, higher than the compression values obtained in the 18DOF model exceeding the pile compression capacity. As a result, the long pile technique configuration does not improve the wind turbine system in terms of stability.

The maximum displacements obtained with MATLAB and SAP2000 are of the same magnitude and appear to be consistent. Table 11 presents the maximum displacements for the vertical- and horizontal-axis wind turbine with the long pile technique applied. The wind transfer function $|H_{wind}(w)|^2$ is also computed to produce the displacement spectral density function in modal coordinates from the spectral density function of the wind force. These spectral density functions are depicted in Figs. 6 and 7 since they differ from the 18-DOF model without the long pile solution.

Table 23
The damped frequencies with the corresponding damping factors for both wind turbines with the 2 MW solution.

VAWT		HAWT	
ζ_i	ω_d (rad/s)	ζ_i	ω_d (rad/s)
0.0500	5.8939	0.0500	5.8363
0.0500	6.1452	0.0500	6.3851
0.0577	10.3939	0.0577	10.5948
0.0618	11.8176	0.0603	11.4804
0.1104	25.0115	0.1045	23.8921
0.1473	34.0833	0.1428	33.5097
0.1712	39.7746	0.1660	39.1404
0.1900	44.1704	0.1813	42.7979
0.2314	53.6361	0.2300	54.1185
0.2348	54.3866	0.2501	58.6698
0.2771	63.6691	0.2713	63.3584
0.2979	68.0756	0.3129	72.2761
0.3182	72.2753	0.3152	72.7441
0.3679	82.0848	0.3748	84.6665
0.3826	84.8492	0.3762	84.9303
0.4044	88.8230	0.3979	88.9874
0.4686	99.5200	0.4496	97.9770
0.4728	100.1513	0.4651	100.4801

Table 24
Maximum displacements in MATLAB and SAP2000 with a 2 MW wind turbine for both types, in meters.

	VAWT			HAWT		
Max displacements [m]	MATLAB	SAP	Error	MATLAB	SAP	Error
u_1	0.00365	0.00801	−0.06%	0.00362	0.00362	−0.06%
u_2	0.00801	0.00802	−0.07%	0.00793	0.00794	−0.07%
u_3	0.01313	0.01315	−0.12%	0.01300	0.01302	−0.11%
u_4	0.01671	0.01674	−0.19%	0.01653	0.01656	−0.19%
u_5	0.01900	0.01898	0.08%	0.01877	0.01876	0.10%
u_6	0.0896	0.0896	0.07%	0.0497	0.0496	0.08%

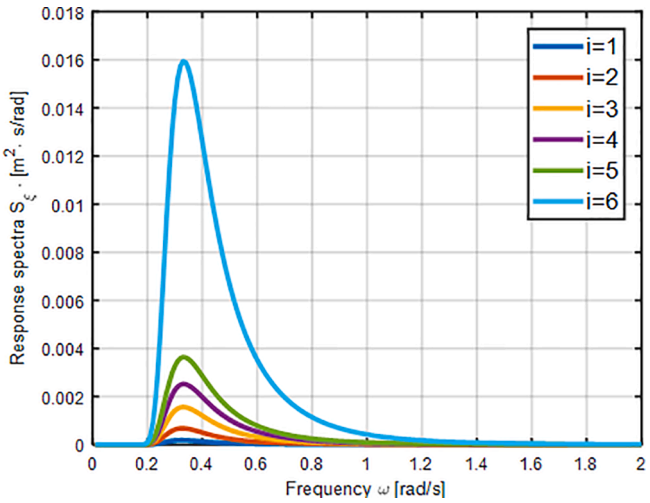

Fig. 23. Response spectra for the displacements in physical coordinates for the 2 MW horizontal-axis wind turbine.

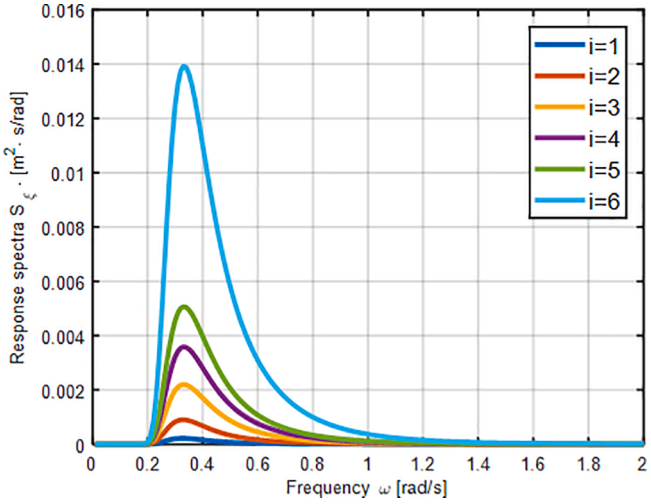

Fig. 24. Response spectra for the displacements in physical coordinates for the 2 MW vertical-axis wind turbine.

As for the 3σ approach, the extreme displacement limit values for the horizontal- and vertical-axis wind turbines, in meters, are presented in Table 12. Comparing the results above, one can conclude that the structure cannot be safe at node 6 at the top of the wind turbine tower because $d_1 = 0.301$ m while d_1 limit $= 0.221$ m for the horizontal-axis wind turbine and $d_1 = 0.410$ m while d_1 limit $= 0.219$ m for the vertical-axis wind turbine.

Table 25
Extreme displacement limit values for horizontal and vertical axis wind turbines, in meters.

	HAWT	VAWT
$3\sigma(\xi_1)$	0.01932	0.02180
$3\sigma(\xi_2)$	0.03837	0.04472
$3\sigma(\xi_3)$	0.05974	0.07102
$3\sigma(\xi_4)$	0.07665	0.09121
$3\sigma(\xi_5)$	0.09222	0.10847
$3\sigma(\xi_6)$	0.194	0.181

Table 26
Results summary for the horizontal- and vertical-axis wind turbine.

		Pile load F_{B1} [kN]	max displacement [m]	3σ approach [m]
HAWT	18-DOF	−17290	0.308	0.149
	Crown Pile	−10416	0.308	0.149
	Long Pile	−20012	0.301	0.221
	Mooring Lines	−17122	0.307	0.144
	Stirrups	−17557	0.301	0.129
	2 MW	−9406	0.0497	0.194
VAWT	18-DOF	−16598	0.410	0.145
	Crown Pile	−10104	0.410	0.144
	Long Pile	−19320	0.410	0.219
	Mooring Lines	−16426	0.409	0.140
	Stirrups	−16865	0.403	0.126
	2 MW	−8106	0.090	0.181

3.3. Mooring lines

The mooring line configuration modifies the 18-DOF model with a mooring line system that links the fourth horizontal plane of the jacket to the seabed in both x and y direction to enhance the stiffness of the structure. The mooring line is modelled with a steel truss element exposed to tension force from environmental loads. Its cross-section diameter is 0.1 m and with a length of 98 m, it develops an angle of 60°with the seafloor. Fig. 8 shows the mooring line configuration. The mass matrix **M** will stay the same as the 18-DOF model [28] and the stiffness matrix **K** will have major changes compared to the 18-DOF model.

For the horizontal- and vertical-axis wind turbines, the undamped natural frequencies and periods are practically the same with differences around 0.01–1 rad/s and 0.01–0.1 s, respectively. The damped frequencies have almost the same values as the 18-DOF model without the retrofitting solution with a difference in damped frequencies around 0.001–0.01 rad/s.

A new applied load at the fourth node of the model related to the tension force in mooring line obtained from SAP2000 is added. Considering Fig. 4 model, the computation of the force in the pile B_1 considers the environmental loads P_i and the horizontal component of

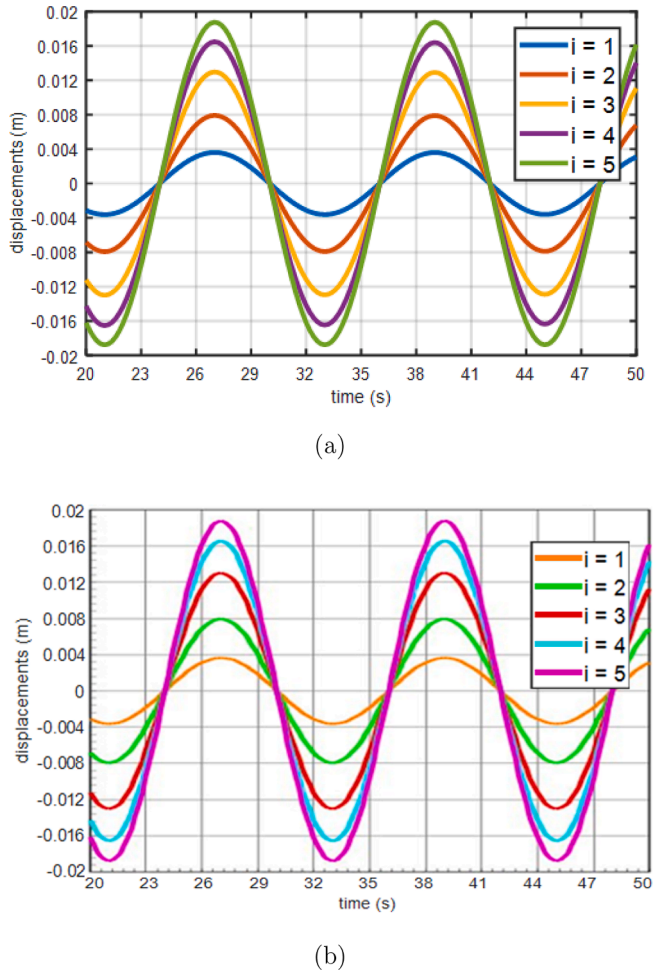

Fig. 19. Response to a harmonic wave and wind force in mass 1 to 5 for the 2 MW horizontal-axis wind turbine in a) MATLAB and b) SAP2000.

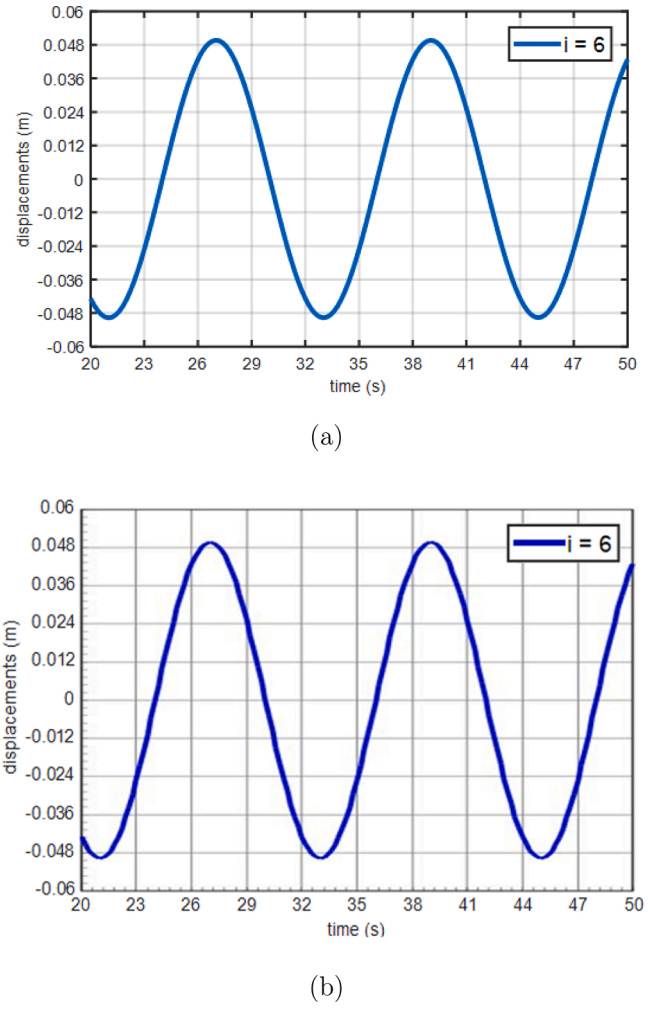

Fig. 20. Response to harmonic wave and wind force for mass 6 for the 2 MW horizontal-axis wind turbine in a) MATLAB and b) SAP2000.

mooring line force, F_{ml}. The maximum compression force in the piles is obtained in B_1 and it is equal to $F_{B1} = -17122$ kN and $F_{B1} = -16426$ kN for the horizontal- and vertical-axis wind turbine, respectively. It is possible to conclude that the compression loads are lower than the pile compression limit but this does not reduce the load in the pile regarding to the wind turbine model. Table 13 presents calculated displacements with MATLAB and SAP2000 for the 18-DOF model with the mooring lines solution and one can conclude that these results are consistent with each other. The displacement spectral density function in terms of physical coordinates is calculated and presented in Figs. 9 and 10.

For the 3σ approach, the extreme displacement limit values for horizontal- and vertical-axis wind turbines with the mooring lines solution, in meters, are presented in Table 14: Table 14 shows that the structure is not safe at top of the wind turbine tower for $d_1 = 0.307$ m while d_1 limit $= 0.144$ m for the horizontal axis wind turbine and $d_1 = 0.409$ m while d_1 limit $= 0.140$ m for the vertical axis wind turbine.

3.4. Stirrups

The stirrups configuration has four extra horizontal stirrups on each side of the jacket structure (18-DOF model). The extra steel elements have sections of $600mm \times 12mm$. Fig. 11,12, shows the 3D model with stirrups in SAP2000:

With the addition of stirrups the mass matrix will suffer some changes and will be as follows (see Table 15). The stiffness matrix also undergoes significant changes. Table 16 shows the eighteen undamped natural frequencies from free vibration for both wind turbines, in rad/s, with the stirrups solution applied. The damped frequencies with the corresponding damping ratios for the horizontal- and vertical-axis wind turbines with stirrups solution are presented in Table 17. The wave load increases due to the added stirrups elements with respect to the 18-DOF model. The wind load remains the same for both wind turbines but the wave forces will have different values, in kN, such as: see Fig. 13–15.

$p_1 = 178250$; $p_2 = 261670$; $p_3 = 442680$; $p_4 = 722890$; $p_5 = 345360$;

As stated previously, the analysis model for the pile force in stirrups configuration (see Fig. 4) is the same and the force in the pile B1, F_{B1}, will be -16865 kN for the vertical-axis wind turbine and -17557 kN for the horizontal-axis wind turbine which will be higher than the values for the 18-DOF model but still lower than the compression capacity of the pile. The following diagrams for the jacket with the stirrups elements added are the results of structural displacements in x direction over a time of 30 s for the lumped masses 1 to 5. The displacement at the wind turbine level is much higher than at other levels, so separate diagrams are plotted as well. Table 18 presents calculated displacements with MATLAB and SAP2000 and one can confirm that they are similar in magnitude.

The wind transfer function, $|H_{wind}(w)|^2$, is also computed to produce displacement spectral density functions in modal coordinates from the spectral density function of the wind force. These spectral densities are depicted in Figs. 16 and 17. In the last step for the 3σ approach, the extreme displacement limit values for the horizontal- and vertical-axis wind turbines with the stirrups elements (in meters) are presented in

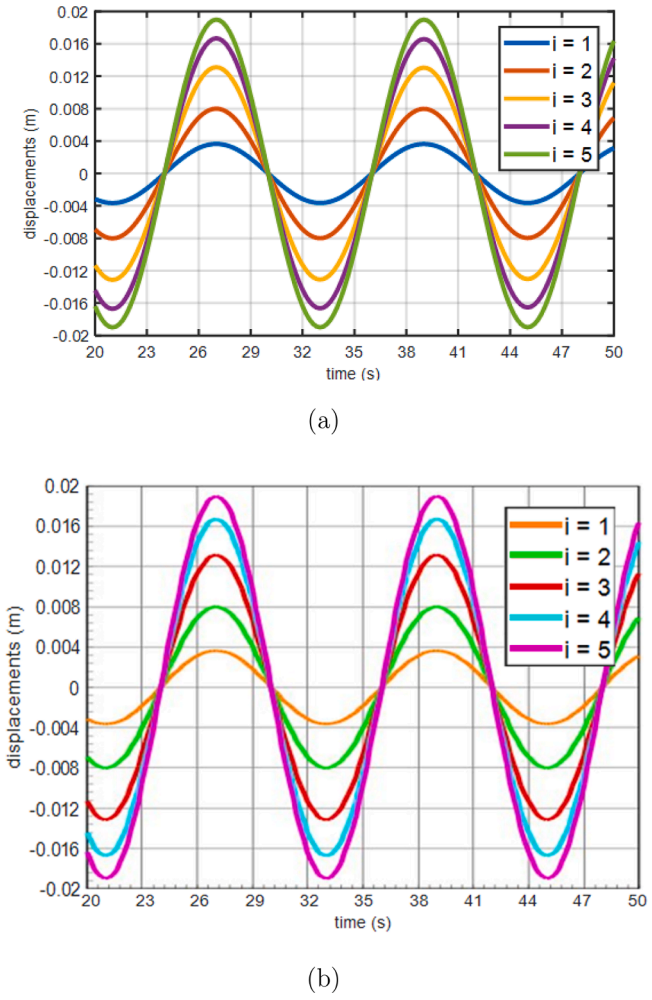

Fig. 21. Response to a harmonic wave and wind force in mass 1 to 5 for the 2 MW vertical-axis wind turbine in a) MATLAB and b) SAP2000.

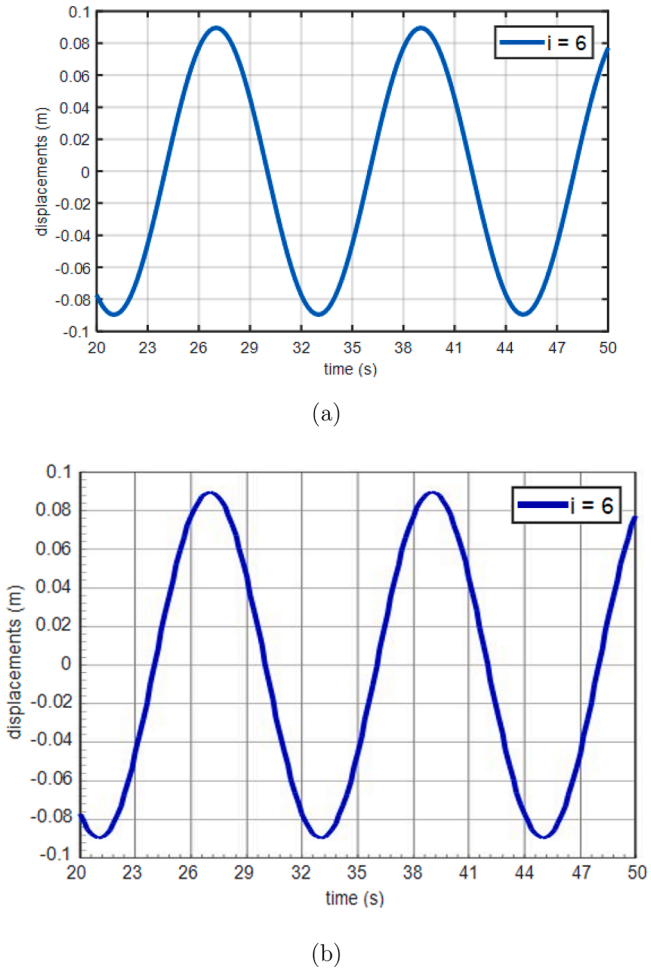

Fig. 22. Response to harmonic wave and wind force for mass 6 for the 2 MW vertical-axis wind turbine in a) MATLAB and b) SAP2000.

Table 19. Table 19 above shows that the structure is not safe at top of the wind tower for $d_1 = 0.301$ m while d_1 limit $= 0.129$ m for the horizontal axis wind turbine and $d_1 = 0.403$ m while d_1 limit $= 0.126$ m for the vertical axis wind turbine.

3.5. 2 MW wind turbine

The 2 MW configuration, unlike the previous techniques, does not introduce intervention in the substructure but on the superstructure focused on the wind turbine tower itself. So instead of a 5 MW turbine, another type of wind tower is considered. The 2 MW turbine employs a smaller steel wind tower and lower mass. For the horizontal-axis wind turbine tower, the tower height is 60 m, the nacelle mass is 57tons, the rotor mass is 23tons and the diameter is 66 m. The wind tower has a truncated-cone shape so at the bottom the diameter is 4 m and the thickness is 0.18 m but at the top the diameter is 3.5 m and the thickness is 0.10 m. As for the vertical-axis wind turbine tower, the tower height is 45 m, the nacelle mass is 57tons, the rotor mass is 147tons and the diameter is 67 m. The wind turbine tower has a cylindrical shape, with a diameter of 4 m and a thickness of 0.2 m. As before, the wind turbine tower is attached to the substructure by the previous concrete transition piece. Fig. 18 shows the jacket structure with a 2 MW turbine solution. The replacement of the wind turbine with a 2 MW changes the mass matrix as is indicated in Table 20. As for the stiffness matrix, in Table 21 there are some changes but they are minimal:

Table 22 shows the eighteen undamped natural frequencies from free vibration for both wind turbines, in rad/s, with the stirrups solution applied. The damped frequencies with the corresponding damping ratios for the horizontal- and vertical-axis 2 MW wind turbines are presented in Table 23. The wave loads are the same as for the 18-DOF model, but the wind load changes due to the different wind turbine tower height and is lower and equal to 838 kN for the horizontal-axis wind turbine and 864 kN for the vertical-axis wind turbine. The analysis model for the pile force with a 2 MW wind turbine is the same (Fig. 4) and the force in the pile B1, F_{B1}, will be −9406 kN for the horizontal-axis wind turbine and −8106 kN for the vertical-axis wind turbine which is lower than for the 18-DOF model and with the other wind turbine configuration and still lower than the compression capacity of the pile. The following diagrams for the jacket with the 2 MW turbine added are the results of structural displacements in the x direction over a time of 30 s for the lumped masses 1 to 5. The displacement at the wind turbine level is much higher than at other levels, so the displacements have been plotted in separate diagrams as well. Table 24 presents the calculated displacements with MATLAB and SAP2000 and it's possible to conclude that it's in the same size of magnitude one can conclude that they are consistent.

The wind transfer function, $|H_{wind}(w)|^2$, was also computed to produce displacement spectral density functions in modal coordinates from spectral density function of the wind force. These spectral densities are depicted in Figs. 23 and 24. As for the 3σ approach, the extreme displacement limit values for the horizontal- and vertical-axis wind turbines with a 2 MW wind turbine for both types, in meters, are presented in Table 25. Table 25 shows that the structure is safe at top of the wind tower for $d_1 = 0.0497$ m while d_1 limit $= 0.194$ m for the

horizontal-axis wind turbine and $d_1 = 0.0896$ m while d_1 limit $= 0.181$ m for the vertical-axis wind turbine.

3.6. Results and discussion

Table 26 displays the summary of the wind turbine towers configurations with the retrofitting solutions for both types of wind turbines: see Fig. 19–22.

The maximum bearing capacity of the pile B1 is $F_{max} = -18000$ kN for both wind turbines. The verification is fulfilled if $F^i_{B1} < F_{max}$ and maximum displacement $< 3\sigma$ values.

It is clear that all retrofitting methods satisfy the pile capacity condition except the long pile configuration and only the 2 MW model fulfills the displacement criteria for the 3σ approach. So the only configuration that is able to satisfy both conditions is the 2 MW wind turbine solution.

4. Concluding remarks

In this research, five different retrofitting solutions are presented, four of which are related to the substructure and one is related to a modified wind turbine. The methods are respectively crown pile configuration, long pile, mooring lines, stirrups and 2 MW configuration. From this work, one can conclude that the safety of the retrofitted models is demonstrated in terms of pile check analysis and the 3σ approach. From all the retrofitting solutions presented, it was concluded that the 2 MW wind turbine solution is the only solution that satisfies the safety conditions. Future studies on offshore structures should emphasize techniques that optimize the rectification costs of the substructures and foundation. More careful analysis of the structure have to take into account different water depths, seabed conditions and metocean conditions that offshore wind farms may be subjected in various sites.

CRediT authorship contribution statement

Paulo Mendes: Conceptualization, Methodology, Formal analysis, Investigation, Data curation, Writing - original draft, Writing - review & editing. **José A.F.O. Correia:** Validation, Investigation, Resources, Writing - review & editing, Visualization, Supervision, Project administration, Funding acquisition. **João Arrojado:** Writing - review & editing. **Taemin Heo:** Writing - review & editing. **Nicholas Fantuzzi:** Methodology, Software, Validation, Investigation, Resources, Writing - original draft, Writing - review & editing, Visualization, Supervision, Project administration, Funding acquisition. **Lance Manuel:** Validation, Resources, Project administration, Funding acquisition.

Declaration of Competing Interest

The authors declare that they have no known competing financial interests or personal relationships that could have appeared to influence the work reported in this paper.

Acknowledgements

The authors wish to ackowledge Marziyeh Zarifkar and Sadegh Takavar for their important contribution in the simulations for this work. Also, the authors wish to acknowledge "Fondazione Flaminia" (Ravenna, Italy) for supporting the present research. Additionally, this research was also supported by national funds (PIDDAC) through the Portuguese Science Foundation (FCT/MCTES); and, base funding - UIDB/04708/2020 and programmatic funding - UIDP/04708/2020 of the CONSTRUCT - Instituto de I&D em Estruturas e Construções - as well as national funds through the FCT/MCTES (PIDDAC). The authors would also like to acknowledge support by UT Austin Portugal Programme and UT-Austin Portugal grants - UTA18-001217 and UTA-EXPL/IET/0111/2019 in support of the project, SOS-WindEnergy, "Sustainable Reuse of Decommissioned Offshore Jacket Platforms for Offshore Wind Energy".

References

[1] Alessi L, Correia JA, Fantuzzi N. Initial design phase and tender designs of a jacket structure converted into a retrofitted offshore wind turbine. Energies 2019;12:659.
[2] Komachi Y, Tabeshpour M, Golafshani A, Mualla I. Retrofit of Ressalat jacket platform (Persian Gulf) using friction damper device. J Zhejiang Univ-Sci A 2011; 12:680–91.
[3] Minh Le L, Van Nguyen D, Chang S, Kim D, Cho SG, Nguyen DD. Vibration control of jacket offshore wind turbine subjected to earthquake excitations by using friction damper. J Struct Integrity Maintenance 2019;4:1–5.
[4] Bossio A, Fabbrocino F, Monetta T, Lignola GP, Prota A, Manfredi G, Bellucci F. Corrosion effects on seismic capacity of reinforced concrete structures. Corros Rev 2019;37:45–56. https://doi.org/10.1515/corrrev-2018-0044.
[5] Bozza A, Asprone D, Fabbrocino F. Urban resilience: A civil engineering perspective. Sustainability 2017;9. https://doi.org/10.3390/su9010103.
[6] R. Morrison, A study of the potential for reuse of north sea oil and gas installations for wind turbines (2016).
[7] D. Gao, C. Zhang, Dynamic behavior of jacket foundation for offshore wind turbine subjected to ship impact, in: EASection 16, Springer, 2021, pp. 719–729.
[8] Cheng Y, Xue Z, Jiang T, Wang W, Wang Y. Numerical simulation on dynamic response of flexible multi-body tower blade coupling in large wind turbine. Energy 2018;152:601–12. https://doi.org/10.1016/j.energy.2018.03.137.
[9] Kaiser MJ, Snyder B. Offshore wind decommissioning regulations and workflows in the Outer Continental Shelf United States. Marine Policy 2012;36:113–21. https://doi.org/10.1016/j.marpol.2011.04.004.
[10] Sørensen EV. Fatigue life of high performance grout in dry and wet environment for wind turbine grouted connections. Nordic Concr Res 2011:1–10.
[11] Schaumann P, Raba A. Systematic testing of the fatigue performance of submerged small-scale grouted joints. In: International Conference on Offshore Mechanics and Arctic Engineering, vol. 56574. American Society of Mechanical Engineers; 2015.
[12] Ziegler L, Muskulus M. Lifetime extension of offshore wind monopiles: Assessment process and relevance of fatigue crack inspection. In: 12th EAWE PhD Seminar. Denmark: DTU Lyngby; 2016.
[13] Zhu S-P, Ai Y, Liao D, Correia JAFO, De Jesus AMP, Wang Q. Recent advances on size effect in metal fatigue under defects: a review. Int J Fract 2021. https://doi.org/10.1007/s10704-021-00526-x.
[14] Xin H, Correia JA, Veljkovic M. Three-dimensional fatigue crack propagation simulation using extended finite element methods for steel grades s355 and s690 considering mean stress effects. Eng Struct 2021;227:111414. https://doi.org/10.1016/j.engstruct.2020.111414.
[15] Xin H, Correia JA, Veljkovic M, Berto F, Manuel L. Residual stress effects on fatigue life prediction using hardness measurements for butt-welded joints made of high strength steels. Int J Fatigue 2021;147:106175. https://doi.org/10.1016/j.ijfatigue.2021.106175.
[16] Zhu S-P, Liu Q, Peng W, Zhang X-C. Computational-experimental approaches for fatigue reliability assessment of turbine bladed disks. Int J Mech Sci 2018;142–143: 502–17. https://doi.org/10.1016/j.ijmecsci.2018.04.050.
[17] Zhu S-P, Liu Q, Yu Z-Y, Liu Y. Fatigue reliability analysis of a turbine disc under multi-source uncertainties. Procedia Struct Integrity 2017;5:967–72. https://doi.org/10.1016/j.prostr.2017.07.137. 2nd International Conference on Structural Integrity, ICSI 2017, 4-7 September 2017, Funchal, Madeira, Portugal.
[18] Niu X-P, Wang R-Z, Liao D, Zhu S-P, Zhang X-C, Keshtegar B. Probabilistic modeling of uncertainties in fatigue reliability analysis of turbine bladed disks. Int J Fatigue 2021;142:105912. https://doi.org/10.1016/j.ijfatigue.2020.105912.
[19] Zhu S-P, Liu Q, Yu Z-Y, Liu Y. Fatigue reliability analysis of a turbine disc under multi-source uncertainties. Procedia Struct Integrity 2017;5:967–72. https://doi.org/10.1016/j.prostr.2017.07.137. 2nd International Conference on Structural Integrity, ICSI 2017, 4-7 September 2017, Funchal, Madeira, Portugal.
[20] Muskulus M, Schafhirt S. Design optimization of wind turbine support structures-a review, Journal of Ocean and Wind. Energy 2014;1:12–22.
[21] Oest J, Sørensen R, Overgaard LCT, Lund E. Structural optimization with fatigue and ultimate limit constraints of jacket structures for large offshore wind turbines. Struct Multidisc Optimiz 2017;55:779–93.
[22] Schafhirt S, Zwick D, Muskulus M, et al. Reanalysis of jacket support structure for computer-aided optimization of offshore wind turbines with a genetic algorithm. In: The Twenty-fourth International Ocean and Polar Engineering Conference. International Society of Offshore and Polar Engineers; 2014.
[23] Yoshida S. Wind turbine tower optimization method using a genetic algorithm. Wind Eng 2006;30:453–69.
[24] Lozano-Minguez E, Kolios AJ, Brennan FP. Multi-criteria assessment of offshore wind turbine support structures. Renewable Energy 2011;36:2831–7.
[25] Saha N, Gao Z, Moan T, Naess A. Short-term extreme response analysis of a jacket supporting an offshore wind turbine. Wind Energy 2014;17:87–104.
[26] O. Catapult, Cost Reduction Monitoring Framework 2016: Summary Report to the Offshore Wind Programme Board, Technical Report, Technical Report, 2017.
[27] A. Ho, A. Mbistrova, G. Corbetta, The European offshore wind industry-key trends and statistics 2015, Brussels, Belgium (2016).
[28] Mendes P, Correia JA, Castro JM, Fantuzzi N, Aidibi A, Manuel L. Horizontal and vertical axis wind turbines on existing jacket platforms: Part 1 - a comparative study. Structures 2021;32:1069–80. https://doi.org/10.1016/j.istruc.2021.01.069.

[29] Schaffer W, Seo J, Choi E, Lee J. Optimized retrofit design of in-service monopile foundation offshore wind turbine transition zone. Eng Struct 2020;220:111001.
[30] E. Skavås, K. Lønvik, A. Pedersen, B. Graver, Review of Design Parameters in DNVGL-RP-B401 Cathodic Protection Design, in: NACE International Corrosion Conference Proceedings, NACE International, 2019, pp. 1–10.
[31] Seo J, Schaffer W, Head M, Shokouhian M, et al. Retrofitting of monopile transition piece for offshore wind turbines. In: The 27th International Ocean and Polar Engineering Conference, International Society of Offshore and Polar Engineers; 2017.
[32] A. Delwiche, I. Tavares, Retrofit strategy using aluminium anodes for the internal sections of windturbine monopiles, in: CORROSION 2017, OnePetro, 2017.
[33] James LCR, Wilson F, Muga Bruce J. Dynamics of Offshore Structures. Wiley 2003.